LETTERS

Quantum entanglement between an optical photon and a solid-state spin qubit

E. Togan[1]*, Y. Chu[1]*, A. S. Trifonov[1], L. Jiang[1,2,3], J. Maze[1], L. Childress[1,4], M. V. G. Dutt[1,5], A. S. Sørensen[6], P. R. Hemmer[7], A. S. Zibrov[1] & M. D. Lukin[1]

Quantum entanglement is among the most fascinating aspects of quantum theory[1]. Entangled optical photons are now widely used for fundamental tests of quantum mechanics[2] and applications such as quantum cryptography[1]. Several recent experiments demonstrated entanglement of optical photons with trapped ions[3], atoms[4,5] and atomic ensembles[6–8], which are then used to connect remote long-term memory nodes in distributed quantum networks[9–11]. Here we realize quantum entanglement between the polarization of a single optical photon and a solid-state qubit associated with the single electronic spin of a nitrogen vacancy centre in diamond. Our experimental entanglement verification uses the quantum eraser technique[5,12], and demonstrates that a high degree of control over interactions between a solid-state qubit and the quantum light field can be achieved. The reported entanglement source can be used in studies of fundamental quantum phenomena and provides a key building block for the solid-state realization of quantum optical networks[13,14].

A quantum network[13] consists of several nodes, each containing a long-lived quantum memory and a small quantum processor, that are connected via entanglement. Its potential applications include long-distance quantum communication and distributed quantum computation[15]. Several recent experiments demonstrated on-chip entanglement of solid-state qubits separated by nanometre[16] to millimetre[17,18] length scales. However, realization of long-distance entanglement based on solid-state systems coupled to single optical photons[19] is an outstanding challenge. The nitrogen-vacancy (NV) centre, a defect in diamond consisting of a substitutional nitrogen atom and an adjacent vacancy, is a promising candidate for implementing a quantum node. The ground state of the negatively charged NV centre is an electronic spin triplet with a 2.88-GHz zero-field splitting between the magnetic sublevels $|m_s=0\rangle$ and $|m_s=\pm1\rangle$ states (from here on denoted $|0\rangle$ and $|\pm1\rangle$). With long coherence times[20], fast microwave manipulation, and optical preparation and detection[21], the NV electronic spin presents a promising qubit candidate. Moreover, it can be coupled to nearby nuclear spins that provide exceptional quantum memories; such coupling allows for the robust implementation of few-qubit quantum registers[16,22]. In this work, we demonstrate the preparation of quantum entangled states between a single photon and the electronic spin of an NV centre:

$$|\Psi\rangle=\frac{1}{\sqrt{2}}(|\sigma_-\rangle|+1\rangle+|\sigma_+\rangle|-1\rangle) \quad (1)$$

where $|\sigma_+\rangle$ and $|\sigma_-\rangle$ are orthogonal circularly polarized single photon states.

The key idea of our experiment is illustrated in Fig. 1a. The NV centre is prepared in a specific excited state ($|A_2\rangle$ in Fig. 1a) that decays with equal probability into two different long lived spin states ($|\pm1\rangle$) by the emission of orthogonally polarized optical photons at 637 nm. The entangled state given by equation (1) is created because photon polarization is uniquely correlated with the final spin state. This entanglement is verified by spin state measurement using a cycling optical transition following the detection of a 637-nm photon of chosen polarization.

Understanding and controlling excited state properties is a central challenge for achieving such a coherent interface between spin memory and optical photons. In contrast to isolated atoms and ions, solid state systems possess complex excited state properties that depend sensitively on their local environment[23]. Non-axial crystal strain is particularly important to the present realization because it affects the optical transitions' selection rules and polarization properties[24].

In the absence of external strain and electric or magnetic fields, properties of the six electronic excited states are determined by the NV centre's C_{3v} symmetry and spin–orbit and spin–spin interactions (shown in Fig. 2a)[24]. Optical transitions between the ground and excited states are spin preserving, but could change electronic orbital angular momentum depending on the photon polarization. Two of the excited states, labelled $|E_x\rangle$ and $|E_y\rangle$ according to their orbital symmetry, correspond to the $m_s=0$ spin projection. Therefore they couple only to the $|0\rangle$ ground state and provide good cycling transitions, suitable for readout of the $|0\rangle$ state population through fluorescence detection. The other four excited states are entangled states of spin and orbital angular momentum. Specifically, the $|A_2\rangle$ state has the form

$$|A_2\rangle=\frac{1}{\sqrt{2}}(|E_-\rangle|+1\rangle+|E_+\rangle|-1\rangle) \quad (2)$$

where $|E_\pm\rangle$ are orbital states with angular momentum projection ±1 along the NV axis. At the same time, the ground states ($|0\rangle$, $|\pm1\rangle$) are associated with the orbital state $|E_0\rangle$ with zero projection of angular momentum (for simplicity, the spatial part of the wavefunction is not explicitly written). Hence, owing to total angular momentum conservation, the $|A_2\rangle$ state decays with equal probability to the $|-1\rangle$ ground state through σ_+ polarized radiation and to $|+1\rangle$ through σ_- polarized radiation.

The inevitable presence of a small strain field, characterized by the strain splitting (Δ_s) of $|E_{x,y}\rangle$, reduces the NV centre's symmetry and shifts the energies of the excited state levels according to their orbital wavefunctions. For moderate and high strain, the excited states are separated into two branches and there is mixing between levels[25]. In the upper branch, an energy gap protects $|A_2\rangle$ against low strain and

[1]Department of Physics, Harvard University, Cambridge, Massachusetts 02138, USA. [2]Department of Physics, California Institute of Technology, Pasadena, California 91125, USA. [3]Institute for Quantum Information, California Institute of Technology, Pasadena, California 91125, USA. [4]Department of Physics and Astronomy, Bates College, Lewiston, Maine 04240, USA. [5]Department of Physics and Astronomy, University of Pittsburgh, Pittsburgh, Pennsylvania 15260, USA. [6]QUANTOP, The Niels Bohr Institute, University of Copenhagen, DK2100 Copenhagen, Denmark. [7]Department of Electrical and Computer Engineering, Texas A&M University, College Station, Texas 77843, USA.
*These authors contributed equally to this work.

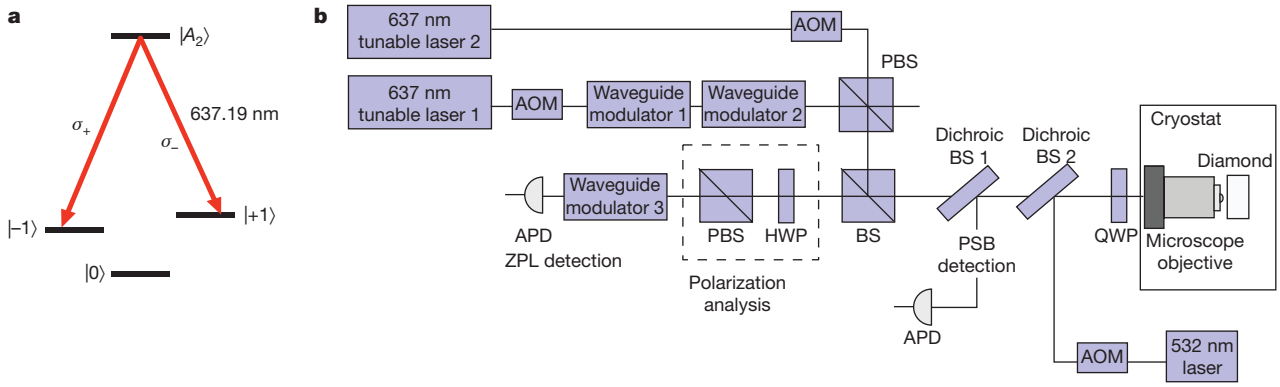

Figure 1 | Scheme for spin-photon entanglement. a, Following selective excitation to the $|A_2\rangle$ state, the Λ-type three level system decays to two different spin states through the emission of orthogonally polarized photons, resulting in spin–photon entanglement. **b**, Schematic of the optical set-up. Individual NV centres are isolated and addressed optically using a microscope objective. Two resonant lasers at 637 nm and an off-resonant laser at 532 nm address various optical transitions. Fluorescence emitted from the NV centre passes through a quarter-wave plate (QWP) and is spectrally separated into PSB and ZPL channels, and detected with avalanche photodiodes (APDs). The latter channel contains entangled photons and is sent using a beam splitter (BS) through a polarization analysis stage consisting of a half-wave plate (HWP) and a polarizing beam splitter (PBS). See text for details.

magnetic fields, preserving the polarization properties of its optical transitions. A group theoretical analysis of the excited states and polarization properties of the transitions is given in the Supplementary Information.

To ensure that $|E_y\rangle$ is a good cycling transition and $|A_2\rangle$ acts as an entanglement generation transition as required for the current study, we select an NV centre with relatively small strain splitting ($\Delta_s \approx 2 \times 1.28$ GHz). Figure 2b presents its excitation spectrum,

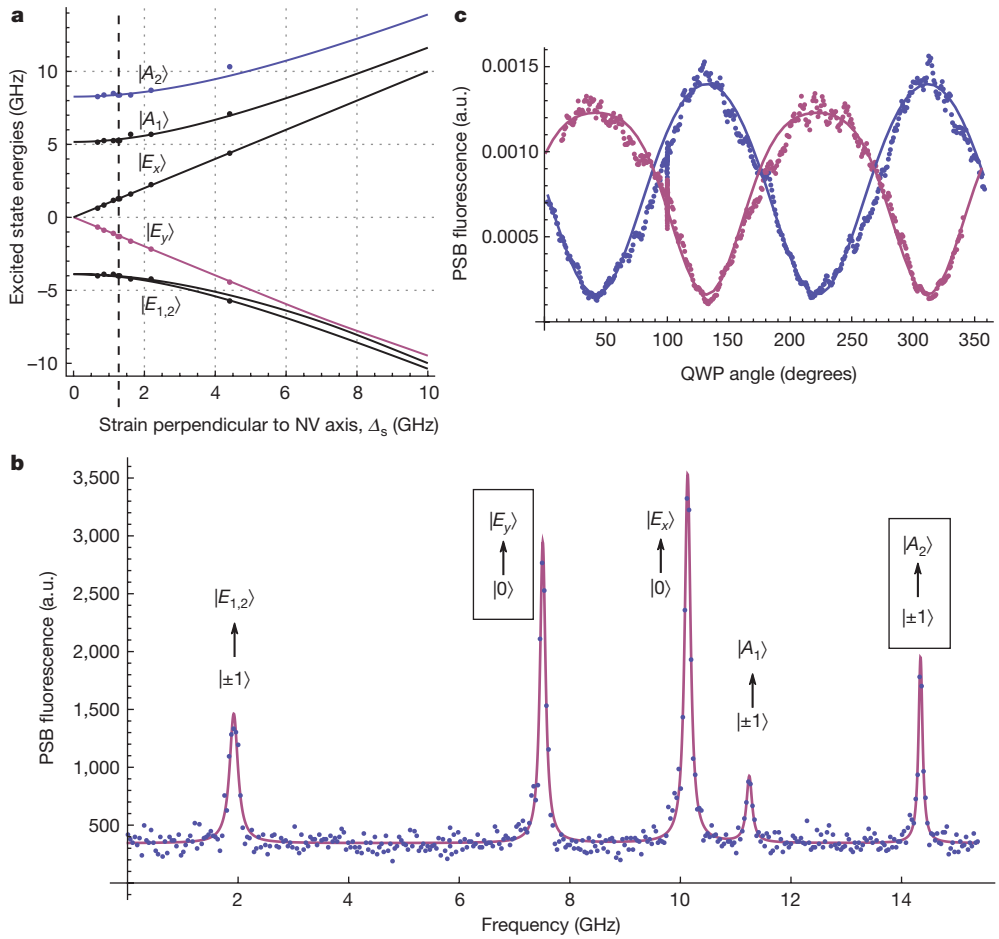

Figure 2 | Characterization of NV centres. a, Energy levels of the NV centre under strain. Solid lines are based on a theoretical model[23] and dots are data from seven NV centres. The dashed line indicates the NV centre used in this paper. **b**, Excitation spectrum of the NV centre under continuous wave (c.w.) microwave radiation. **c**, Polarization properties of the $|\pm1\rangle \rightarrow |A_2\rangle$ transition in absorption. The system is initially prepared in $|+1\rangle$ (blue) or $|-1\rangle$ (red). We then apply a laser pulse of varying polarization to the $|A_2\rangle$ state while collecting fluorescence. Oscillations with visibility 77 ± 10% indicate that the transitions linking $|\pm1\rangle$ to $|A_2\rangle$ are circularly polarized and mutually orthogonal (see Supplementary Information for details).

while Fig. 2c demonstrates the desired polarization properties of the $|\pm1\rangle \leftrightarrow |A_2\rangle$ transitions via resonant excitation.

We now turn to the experimental demonstration of spin–photon entanglement. Our experimental set-up is outlined in Fig. 1b and described in the Supplementary Information. To create the entangled state, we use coherent emission within the narrow-band zero phonon line (ZPL), which includes only 4% of the NV centre's total emission. The remaining optical radiation occurs in the frequency shifted phonon side band (PSB), which is accompanied by phonon emission that causes deterioration of the spin–photon entanglement[26]. Isolating the weak ZPL emission presents a significant experimental challenge owing to strong reflections of the resonant excitation pulse reaching the detector. By exciting the NV centre with a circularly polarized 2-ns π-pulse that is shorter than the emission timescale, we can use detection timing to separate reflection from fluorescence photons. A combination of confocal rejection, modulators and finite transmittivity of our optics suppresses the reflections sufficiently to clearly detect the NV centre's ZPL emission in a 20-ns region (Fig. 3).

For photon state determination, ZPL photons in either the $|\sigma_\pm\rangle$ or $|H\rangle = \frac{1}{\sqrt{2}}(|\sigma_+\rangle + |\sigma_-\rangle)$, $|V\rangle = \frac{1}{\sqrt{2}}(|\sigma_+\rangle - |\sigma_-\rangle)$ basis are selected by a polarization analysis stage and detected after an optical path of ~2 m. Spin readout then occurs after a 0.5-μs spin memory interval following photon detection by transferring population from either the $|\pm1\rangle$ states or from their appropriately chosen superposition into the $|0\rangle$ state using microwave pulses, $\Omega_{\pm1}$. The pulses selectively address the $|0\rangle \leftrightarrow |\pm1\rangle$ transitions with resonant frequencies $\omega_\pm$ that differ by $\delta\omega = \omega_+ - \omega_- = 122$ MHz due to an applied magnetic field. For superpositions of $|\pm1\rangle$ states, an echo sequence is applied before the state transfer to extend the spin coherence time (see Supplementary Information). The transfer is followed by resonant excitation of the $|0\rangle \leftrightarrow |E_y\rangle$ transition and collection of the PSB fluorescence. We carefully calibrate the transferred population measured in the $|0\rangle$ state using the procedure detailed in Methods.

Figure 4a shows the populations in the $|\pm1\rangle$ states, measured conditionally on the detection of a single circularly polarized ZPL photon. Excellent correlations between the photon polarization and NV spin states are observed.

To complete the verification of entanglement, we now show that correlations persist when ZPL photons are detected in a rotated polarization basis. On detection of a linearly polarized $|H\rangle$ or $|V\rangle$ photon at time t_d, the entangled state in equation (1) is projected to $|\pm\rangle = \frac{1}{\sqrt{2}}(|+1\rangle \pm |-1\rangle)$, respectively. These states subsequently evolve in time (t) according to:

$$|\pm\rangle_t = \frac{1}{\sqrt{2}}\left(e^{-i\omega_+(t-t_d)}|+1\rangle \pm e^{-i\omega_-(t-t_d)}|-1\rangle\right) \quad (3)$$

In order to read out the relative phase of superposition states between $|+1\rangle$ and $|-1\rangle$, we use two resonant microwave fields with frequencies ω_+ and ω_- to coherently transfer the state $|M\rangle = \frac{1}{\sqrt{2}}\left(e^{-i\omega_+ t}|+1\rangle + e^{-i(\omega_- t - (\phi_+ - \phi_-))}|-1\rangle\right)$ to $|0\rangle$ (see Fig. 3b), where the initial relative phase $\phi_+ - \phi_-$ is set to the same value for each round of the experiment. Thus, the conditional probability of measuring the state $|M\rangle$ is

$$p_{M|H,V}(t_d) = \frac{1 \pm \cos\alpha(t_d)}{2} \quad (4)$$

where $\alpha(t_d) = (\omega_+ - \omega_-)t_d + (\phi_+ - \phi_-)$. Equation (4) indicates that the two conditional probabilities should oscillate with a π phase difference as a function of the photon detection time, t_d. This can be understood as follows. In the presence of Zeeman splitting ($\delta\omega \neq 0$), the NV centre's spin state is entangled with both the polarization and frequency of the emitted photon. The photon's frequency provides which-path information about its decay. In the spirit of quantum eraser techniques, the detection of $|H\rangle$ or $|V\rangle$ at t_d with high time resolution (~300 ps $\ll 1/\delta\omega$) erases the frequency information[5,12]. When the initial relative phase between the microwave fields $\Omega_{\pm1}$

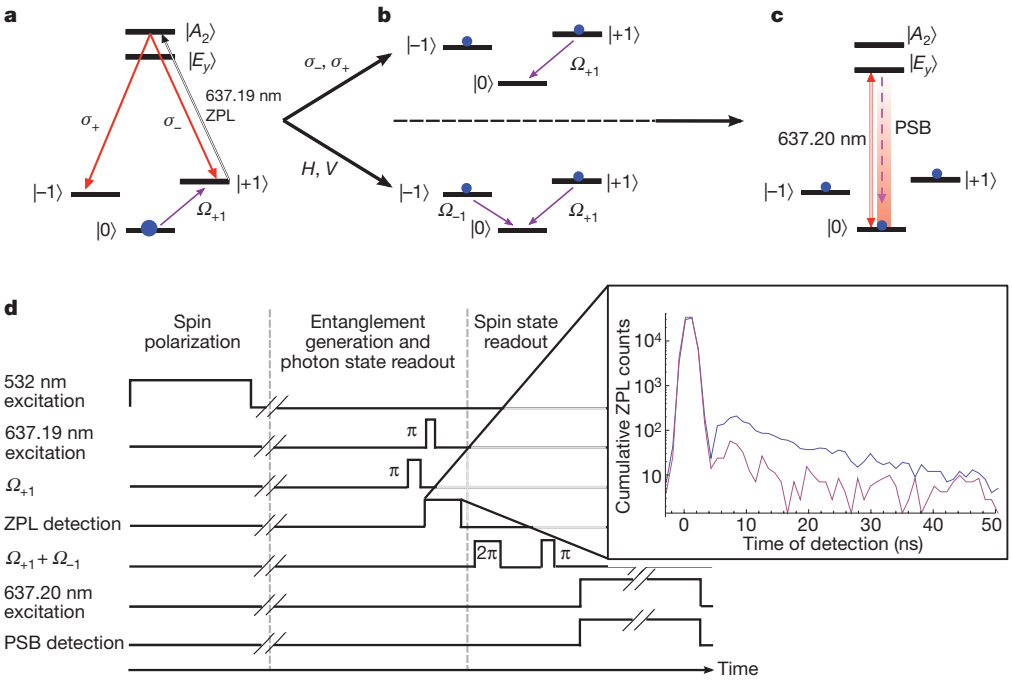

Figure 3 | Experimental procedure for entanglement generation. **a**, After spin polarization into $|0\rangle$, population is transferred to $|+1\rangle$ by a microwave π-pulse (Ω_{+1}). The NV is excited to $|A_2\rangle$ with a 637.19-nm π-pulse and the ZPL emission is collected. **b**, If a σ_+ or σ_- photon is detected, the population in $|+1\rangle$ or $|-1\rangle$ is transferred to $|0\rangle$. If an $|H\rangle$ or $|V\rangle$ photon is detected, a τ–2π–τ echo sequence (see Supplementary Information) is applied with Ω_{+1} and Ω_{-1}, followed by a π-pulse which transfers the population in $|M\rangle$ (see text) to $|0\rangle$. **c**, The population in $|0\rangle$ is measured using the 637.20-nm optical readout transition. **d**, Pulse sequence for the case where an $|H\rangle$ or $|V\rangle$ ZPL photon is detected (time axis not to scale). If a $\sigma_\pm$ photon is detected instead, only a π-pulse on either Ω_{+1} or Ω_{-1} is used for spin readout. Inset, detection time of ZPL channel photons, showing reflection from diamond surface and subsequent NV emission (blue) and background counts (purple).

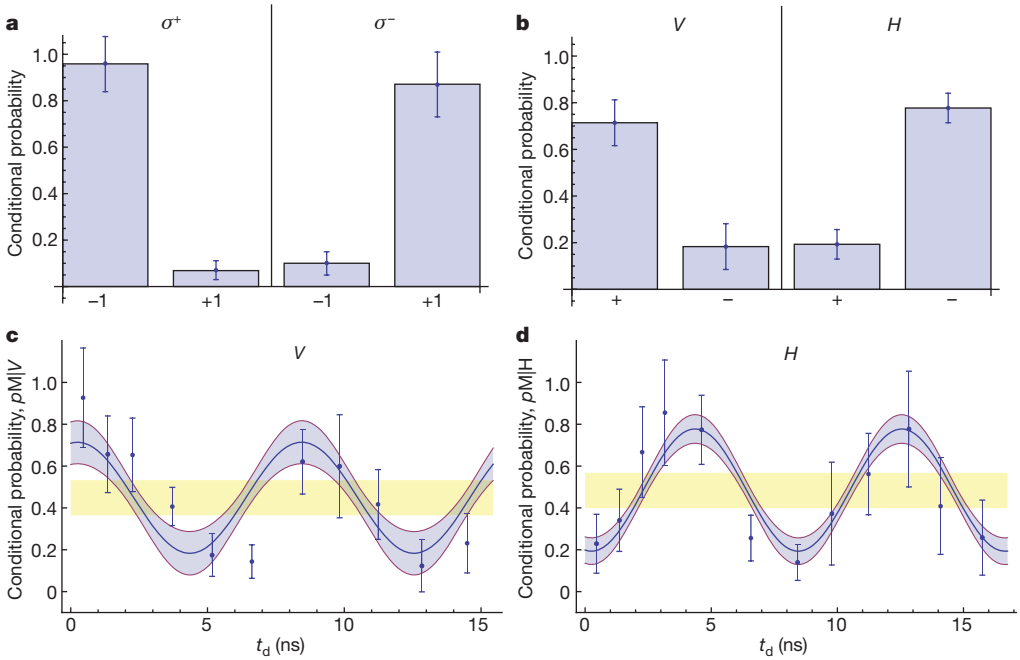

Figure 4 | Measurement of spin-photon correlations in two bases. **a**, Conditional probability of measuring $|\pm 1\rangle$ after the detection of a $\sigma+$ or $\sigma-$ photon. **b**, Conditional probability of measuring $|\pm\rangle$ after the detection of an H or V photon, extracted from a fit to data shown in **c** and **d**. **c**, **d**, Measured conditional probability of finding the electronic spin in the state $|M\rangle$ after detection of a V (**c**) or H (**d**) photon at time t_d. Blue shaded region is the 68% confidence interval for the fit (solid line) to the time-binned data (Supplementary Information). Errors bars on data points show ± 1 s.d. Combined with the data shown in **a**, oscillations with amplitude outside of the yellow regions result in fidelities greater than 0.5. The visibility of the measured oscillations are 0.59 ± 0.18 (**c**) and 0.60 ± 0.11 (**d**).

is kept constant, the acquired phase difference $(\omega_+ - \omega_-)t_d$ gives rise to oscillations in the conditional probability and produces an effect equivalent to varying the relative phase in the measured superposition; this allows us to verify the coherence of the spin–photon entangled state.

The detection times of ZPL photons are recorded during the experiment without any time gating, which allows us to study spin–photon correlations without reducing the count rate. The resulting data are analysed in two different ways. First, we time-bin the data and use it to evaluate the conditional probabilities of measuring spin state $|M\rangle$ as a function of $|H\rangle$ or $|V\rangle$ photon detection time (Fig. 4c, d). Off-diagonal elements of the spin–photon density matrix are evaluated from a simultaneous fit to the binned data (see Methods). The time bins are chosen to minimize fit uncertainty, as described in Supplementary Information. The resulting conditional probabilities are used to evaluate a lower bound on the entanglement fidelity of $F \geq 0.69 \pm 0.068$, above the classical limit of 0.5, indicating the preparation of an entangled state.

We further reinforce our analysis using the method of maximum likelihood estimate. As described in Supplementary Information, this method is applied to raw, un-binned ZPL photon detection and spin measurement data and yields a probability distribution of a lower bound on the fidelity. Consistent with the time-binned approach, we find that our data are described by a near Gaussian probability distribution associated with a fidelity of $F \geq 0.70 \pm 0.070$ (see Supplementary Fig. 7). Significantly, the cumulative probability distribution directly shows that the measured lower bound on the fidelity is above the classical limit with a probability of 99.7%.

Several experimental imperfections reduce the observed entanglement fidelity. First, the measured strain and magnetic field slightly mixes the $|A_2\rangle$ state with the other excited states. On the basis of Fig. 2b, we estimate that the $|A_2\rangle$ state imperfection and photon depolarization in the set-up together reduce the fidelity by 12%, the latter being the dominant effect. Imperfections in readout and echo microwave pulses decrease the fidelity by 3%. Other error sources include finite signal to noise ratio in the ZPL channel (fidelity decrease 11%), as well as timing jitter (another 4%). The resulting expected fidelity (75%) is consistent with our experimental observations. Finally, the entanglement generation succeeds with probability $p \approx 10^{-6}$, which is limited by low collection and detection efficiency as well as the small probability of ZPL emission.

Entanglement of pairs of remote quantum registers is one important potential application of the technique described here[11]. This can be done by coincidence measurements on a pair of photons emitted by two remote NV centres. The key figure of merit for such an entanglement operation over a distance L is proportional to $p^2 \frac{\gamma T}{1+\gamma\tau}$, where $\gamma \approx 2\pi \times 15$ MHz is the spontaneous decay rate of the NV centre, $\tau = L/c$ is the photon travel time, c is the velocity of light, and T is the memory lifetime. A large figure of merit is critical for applications such as quantum repeaters and entanglement purification protocols. The 0.5-μs spin memory interval in our experiments can be extended to several hundred microseconds using spin echo techniques. Furthermore, by mapping the electronic spin state onto proximal nuclei, T can be extended to hundreds of milliseconds[22]. The key limitation in attaining a large figure of merit is low p. It can be circumvented if optical cavities are used, which simultaneously enhances emission into the ZPL and improves collection efficiency through integration with appropriate waveguides. For example, by using a photonic crystal nanocavity[27–29], the potential rate for spin–spin entanglement generation can be about 1 MHz for $\tau < 1/\gamma$ and a few hertz for τ corresponding to $L \approx 100$ km, resulting in $p^2 \frac{\gamma T}{1+\gamma\tau} \geq 1$. Beyond this specific application, our ability to control interactions between NV centres and quantum light fields demonstrates that quantum optical techniques, such as all-optical spin control, non-local entanglement[11] and photon storage[30], can be implemented using long-lived solid-state qubits, paving the way for a wide variety of potential applications in quantum optics and quantum information science.

METHODS SUMMARY

Spin readout. We determine the spin of the NV centre by resonantly exciting the $|0\rangle \leftrightarrow |E_y\rangle$ transition and collecting emission on the PSB within a 10-μs window. To obtain accurate readout levels relevant for calibration of our experimental data, we effectively project the state of the NV centre into $|0\rangle$ or $|\pm 1\rangle$ before spin measurement by detecting a PSB photon after exciting to the $|E_y\rangle$ or $|A_2\rangle$ state, respectively. Subsequent readout produces a maximum number of 0.11 ± 0.0022 counts per shot when the NV is initially in the $|0\rangle$ state and a minimum number (consistent with background) when it is in the $|\pm 1\rangle$ states. These levels are then used to calculate the populations measured for entanglement verification. Compared to conventional spin measurements in NV centres, this method is less sensitive to effects such as imperfect initial spin polarization, NV photo-ionization, and spectral or spatial instabilities. A detailed description of the spin readout measurement and calibration is given in the Supplementary Information.

Calculation of entanglement fidelity. To estimate the entanglement fidelity, we first use the conditional measurement shown in Fig. 4a, b to determine diagonal elements of the spin–photon density matrix in the $|\sigma_\pm\rangle, |\pm 1\rangle$ basis. As $\sigma_\pm$ photons are emitted with equal probability (see Supplementary Information), we find $\rho_{\sigma_+ -1,\sigma_+ -1} = \frac{1}{2}p_{-1|\sigma_+} = \frac{1}{2}(0.96 \pm 0.12)$, $\rho_{\sigma_+ +1,\sigma_+ +1} = \frac{1}{2}(0.07 \pm 0.04)$, $\rho_{\sigma_- -1,\sigma_- -1} = \frac{1}{2}(0.10 \pm 0.05)$, and $\rho_{\sigma_- +1,\sigma_- +1} = \frac{1}{2}(0.87 \pm 0.14)$. To evaluate the off-diagonal elements, we rotate the measurement basis by projecting the photon to the $|H\rangle$ or $|V\rangle$ states and measuring the conditional probability of being in state $|M\rangle$, which is equal to $|\pm\rangle$ for particular choices of α (for example, $|+\rangle = |M\rangle_{|\alpha=0}$). The required diagonal matrix elements in the $|H\rangle, |V\rangle, |\pm\rangle$ basis are then given by $\rho_{V+,V+} = \frac{1}{2}p_{M|V}(\alpha = 0)$, and similarly for $\rho_{H+,H+}, \rho_{H-,H-}$ and $\rho_{V-,V-}$. We model the experimentally measured conditional probabilities with the forms $p_{M|H} = (b_H + a_H \cos\alpha)/2$ and $p_{M|V} = (b_V - a_V \cos\alpha)/2$, where $b_{H,V}$ are the offsets of the oscillations and $a_{H,V}$ are their amplitudes. Using a simultaneous fit to the data in Fig. 4c, d that constrains the frequency to be the Zeeman splitting, we obtain the values $\rho_{V+,V+} - \rho_{V-,V-} = a_V/2 = \frac{1}{2}(0.53 \pm 0.16)$, $\rho_{H-,H-} - \rho_{H+,H+} = a_H/2 = \frac{1}{2}(0.58 \pm 0.10)$ The information obtained is sufficient to provide a lower bound for the entanglement fidelity. Using the analysis in ref. 3 $F \geq \frac{1}{2}(\rho_{\sigma_+ -1,\sigma_+ -1} + \rho_{\sigma_- +1,\sigma_- +1} - 2\sqrt{\rho_{\sigma_+ +1,\sigma_+ +1}\rho_{\sigma_- -1,\sigma_- -1}} + \rho_{V+,V+} - \rho_{V-,V-} + \rho_{H-,H-} - \rho_{H+,H+})$, we find $F \geq 0.69 \pm 0.068$. This analysis agrees with the results of an independent maximum likelihood analysis described in the Supplementary Information, which yields a near Gaussian probability distribution for a lower bound on the fidelity with $F \geq 0.70 \pm 0.070$.

Full Methods and any associated references are available in the online version of the paper at www.nature.com/nature.

Received 8 February; accepted 8 June 2010.

1. Nielsen, M. A. & Chuang, I. L. *Quantum Computation and Quantum Information* (Cambridge Univ. Press, 2000).
2. Aspect, A., Grangier, P. & Roger, G. Experimental realization of Einstein-Podolsky-Rosen-Bohm Gedankenexperiment: a new violation of Bell's inequalities. *Phys. Rev. Lett.* **49,** 91–94 (1982).
3. Blinov, B. B., Moehring, D. L., Duan, L. M. & Monroe, C. Observation of entanglement between a single trapped atom and a single photon. *Nature* **428,** 153–157 (2004).
4. Volz, J. *et al.* Observation of entanglement of a single photon with a trapped atom. *Phys. Rev. Lett.* **96,** 030404 (2006).
5. Wilk, T., Webster, S. C., Kuhn, A. & Rempe, G. Single-atom single-photon quantum interface. *Science* **317,** 488–490 (2007).
6. Yuan, Z.-S. *et al.* Experimental demonstration of a BDCZ quantum repeater node. *Nature* **454,** 1098–1101 (2008).
7. Matsukevich, D. *et al.* Entanglement of a photon and a collective atomic excitation. *Phys. Rev. Lett.* **95,** 040405 (2005).
8. Sherson, J. F. *et al.* Quantum teleportation between light and matter. *Nature* **443,** 557–560 (2006).
9. Cabrillo, C., Cirac, J. I., Garcia-Fernandez, P. & Zoller, P. Creation of entangled states of distant atoms by interference. *Phys. Rev. A* **59,** 1025–1033 (1999).
10. Chou, C. W. *et al.* Measurement-induced entanglement for excitation stored in remote atomic ensembles. *Nature* **438,** 828–832 (2005).
11. Moehring, D. L. *et al.* Entanglement of single-atom quantum bits at a distance. *Nature* **449,** 68–71 (2007).
12. Scully, M. O. & Drühl, K. Quantum eraser: a proposed photon correlation experiment concerning observation and "delayed choice" in quantum mechanics. *Phys. Rev. A* **25,** 2208–2213 (1982).
13. Kimble, H. J. The quantum internet. *Nature* **453,** 1023–1030 (2008).
14. Childress, L., Taylor, J. M., Sørensen, A. S. & Lukin, M. D. Fault-tolerant quantum communication based on solid-state photon emitters. *Phys. Rev. Lett.* **96,** 070504 (2006).
15. Duan, L.-M. & Monroe, C. Robust quantum information processing with atoms, photons, and atomic ensembles. *Adv. At. Mol. Opt. Phys.* **55,** 419–464 (2008).
16. Neumann, P. *et al.* Multipartite entanglement among single spins in diamond. *Science* **320,** 1326–1329 (2008).
17. Ansmann, M. *et al.* Violation of Bell's inequality in Josephson phase qubits. *Nature* **461,** 504–506 (2009).
18. DiCarlo, L. *et al.* Demonstration of two-qubit algorithms with a superconducting quantum processor. *Nature* **460,** 240–244 (2009).
19. de Riedmatten, H., Afzelius, M., Staudt, M. U., Simon, C. & Gisin, N. A solid-state light-matter interface at the single-photon level. *Nature* **456,** 773 (2008).
20. Balasubramanian, G. *et al.* Ultralong spin coherence time in isotopically engineered diamond. *Nature Mater.* **8,** 383–387 (2009).
21. Fuchs, G. D., Dobrovitski, V. V., Toyli, D. M., Heremans, F. J. & Awschalom, D. D. Gigahertz dynamics of a strongly driven single quantum spin. *Science* **326,** 1520–1522 (2009).
22. Dutt, M. V. G. *et al.* Quantum register based on individual electronic and nuclear spin qubits in diamond. *Science* **316,** 1312–1316 (2007).
23. Tamarat, P. *et al.* Spin-flip and spin-conserving optical transitions of the nitrogen-vacancy centre in diamond. *N. J. Phys.* **10,** 045004 (2008).
24. Manson, N., Harrison, J. & Sellars, M. Nitrogen-vacancy center in diamond: model of the electronic structure and associated dynamics. *Phys. Rev. B* **74,** 104303 (2006).
25. Santori, C. *et al.* Coherent population trapping of single spins in diamond under optical excitation. *Phys. Rev. Lett.* **97,** 247401 (2006).
26. Kaiser, F. *et al.* Polarization properties of single photons emitted by nitrogen-vacancy defect in diamond at low temperature. ⟨http://arXiv.org/abs/0906.3426⟩ (2009).
27. Englund, D., Faraon, A., Fushman, I., Stoltz, N. & Petroff, P. Controlling cavity reflectivity with a single quantum dot. *Nature* **450,** 857–861 (2007).
28. Schietinger, S., Schröder, T. & Benson, O. One-by-one coupling of single defect centers in nanodiamonds to high-Q modes of an optical microresonator. *Nano Lett.* **8,** 3911–3915 (2008).
29. Wang, C. F. *et al.* Fabrication and characterization of two-dimensional photonic crystal microcavities in nanocrystalline diamond. *Appl. Phys. Lett.* **91,** 201112 (2007).
30. Fleischhauer, M., Imamoğlu, A. & Marangos, J. P. Electromagnetically induced transparency: optics in coherent media. *Rev. Mod. Phys.* **77,** 633–673 (2005).

Supplementary Information is linked to the online version of the paper at www.nature.com/nature.

Acknowledgements We thank F. Jelezko, J. Wrachtrup, V. Jacques, N. Manson, J. Taylor and J. MacArthur for discussions and experimental help. This work was supported by the Defense Advanced Research Projects Agency, NSF, Harvard-MIT CUA, the NDSEG Fellowship and the Packard Foundation. The content of the information does not necessarily reflect the position or the policy of the US Government, and no official endorsements should be inferred.

Author Contributions All authors contributed extensively to the work presented in this paper.

Author Information Reprints and permissions information is available at www.nature.com/reprints. The authors declare no competing financial interests. Readers are welcome to comment on the online version of this article at www.nature.com/nature. Correspondence and requests for materials should be addressed to M.D.L. (lukin@fas.harvard.edu).

METHODS

Experimental set-up. Our experiments are performed using a natural bulk diamond sample kept below 7 K. A Nikon 0.95 NA microscope objective is used in our confocal set-up to address individual NV centres. Resonant excitation of the readout and entanglement generation transitions are done using two external cavity diode lasers. To overcome the main experimental challenge of ensuring sufficient signal to noise of the detected ZPL emission, we eliminate background from laser light reflected off the diamond surface by creating an isolated excitation π-pulse using two cascaded waveguide modulators. This excitation pulse is sent through a quarter-wave plate that is fixed during all experimental runs to produce the circular polarization that most efficiently excites the NV to the $|A_2\rangle$ state. We note that, because our measurements are conditioned on the detection of an emitted photon, optical π-pulse imperfections only affect the efficiency of the entanglement generation and not the measured fidelity. In the collection path, the ZPL is sent to a polarization analysis set-up consisting of an HWP and a PBS for photon state selection. It then passes through a narrow frequency filter before being detected by a low dark count APD. We use a waveguide based electro-optical modulator before the APD to further reduce reflections of the excitation pulse and suppress detector afterpulsing. Special care is taken to minimize reflections during the measurement window to around the dark count level of the detector.

Addressing of the $|0\rangle \leftrightarrow |\pm 1\rangle$ microwave transitions is carried out using a 15-μm copper wire attached to the diamond. For simultaneous addressing, two microwave fields (generated by mixing the difference frequency of the two transitions with their average frequency) are separated using bandpass filters, individually attenuated, and recombined to balance their power. Low shot-to-shot noise in the microwave fields' relative phase is crucial. This is achieved by triggering all timing-sensitive channels from one output event of a controller device that produces the entanglement generation and conditioned readout sequences. Timing information of both ZPL and PSB photons are collected by combining them at the input of a time-tagged-single-photon-counting device.

Given an experiment repetition rate of $\sim$100 kHz and an entanglement generation success probability of $p \approx 10^{-6}$, we then detect on average one signal photon every few seconds. As the microwave π-pulses used for population transfer to the $|0\rangle$ state are nearly perfect and about 100 repetitions are required for reliable spin state determination, roughly 24 h of data taking were required for each of the four photon polarizations measured. Overall, characterization, calibration, and data acquisition for a given NV centre were performed over a roughly two month period. The overall measurement time for each individual NV centre is limited by the long term mechanical stability of the set-up.